UC Davis

UC Davis Previously Published Works

Title

Molecular mechanism of poliovirus Sabin vaccine strain attenuation

Permalink

https://escholarship.org/uc/item/5jp339bn

Journal

Journal of Biological Chemistry, 293(40)

ISSN

0021-9258

Authors

Avanzino, Brian C

Jue, Helen

Miller, Clare M

et al.

Publication Date

2018-10-01

DOI

10.1074/jbc.ra118.004913

Copyright Information

This work is made available under the terms of a Creative Commons Attribution License, available at https://creativecommons.org/licenses/by/4.0/

Peer reviewed

eScholarship.org Powered by the California Digital Library
University of California

Molecular mechanism of poliovirus Sabin vaccine strain attenuation

Received for publication, July 17, 2018, and in revised form, August 11, 2018 Published, Papers in Press, August 20, 2018, DOI 10.1074/jbc.RA118.004913

Brian C. Avanzino[‡], Helen Jue[‡1], Clare M. Miller[§], Emily Cheung[§1], Gabriele Fuchs[§2], and Christopher S. Fraser[‡3]

From the [‡]Department of Molecular and Cellular Biology, College of Biological Sciences, University of California, Davis, California 95616 and the [§]Department of Biological Sciences, The RNA Institute, University at Albany, State University of New York, Albany, New York 12222

Edited by Charles E. Samuel

Recruitment of poliovirus (PV) RNA to the human ribosome requires the coordinated interaction of the viral internal ribosome entry site (IRES) and several host cellular initiation factors and IRES *trans*-acting factors (ITAFs). Attenuated PV Sabin strains contain point mutations in the PV IRES domain V (dV) that inhibit viral translation. Remarkably, attenuation is most apparent in cells of the central nervous system, but the molecular basis to explain this is poorly understood. The dV contains binding sites for eukaryotic initiation factor 4G (eIF4G) and polypyrimidine tract–binding protein (PTB). Impaired binding of these proteins to the mutant IRESs has been observed, but these effects have not been quantitated. We used a fluorescence anisotropy assay to reveal that the Sabin mutants reduce the equilibrium dissociation constants of eIF4G and PTB to the PV IRES by up to 6-fold. Using the most inhibitory Sabin 3 mutant, we used a real-time fluorescence helicase assay to show that the apparent affinity of an active eIF4G/4A/4B helicase complex for the IRES is reduced by 2.5-fold. The Sabin 3 mutant did not alter the maximum rate of eIF4A-dependent helicase activity, suggesting that this mutant primarily reduces the affinity, rather than activity, of the unwinding complex. To confirm this affinity model of attenuation, we show that eIF4G overexpression in HeLa cells overcomes the attenuation of a Sabin 3 mutant PV–luciferase replicon. Our study provides a quantitative framework for understanding the mechanism of PV Sabin attenuation and provides an explanation for the previously observed cell type–specific translational attenuation.

The oral polio vaccine consists of a live attenuated virus and has been essential in the global effort to eradicate poliovirus (PV).[4] The Sabin strains comprising the vaccine were generated by serial passage of the three major PV strains in nonhuman primates and cultured primate cells, resulting in strains with reduced neurovirulence (1–3). The major genetic determinants of all three Sabin strains have been mapped to mutations in the 5′ UTR of the genomic PV RNA in a region named the internal ribosome entry site (IRES) and result in reduced levels of viral translation (4–8). The PV IRES translates the genomic viral RNA through a cap-independent mechanism by hijacking the cellular translation machinery. A key step in PV translation involves the binding of eukaryotic initiation factor 4G (eIF4G) to PV IRES domain V (dV), which is located near the 3′ border of the IRES (Fig. 1) (9). An important function of eIF4G is to recruit eIF4A, an RNA-dependent DEAD-box helicase, to the IRES (9). This helicase functions to restructure the IRES to promote ribosome recruitment. The eIF4A accessory protein eIF4B also binds PV dV and stimulates PV translation initiation (10). In addition to canonical translation initiation factors, the PV IRES requires noncanonical cellular RNA-binding proteins called IRES *trans*-acting factors. These include polypyrimidine tract–binding protein (PTB), La autoantigen, and poly(rC)-binding protein 2 (PCBP2) (11–14). Interestingly, PTB binds to PV dV, and the binding sites of the central core of eIF4G and PTB appear to overlap (9, 15, 16). Thus, the recruitment of both canonical translation initiation factors and noncanonical IRES *trans*-acting factors to the IRES represent a key step preceding ribosome recruitment and PV translation.

The key attenuating Sabin mutations have been mapped to PV dV at nucleotides 480, 481, and 472 in the Sabin 1, Sabin 2, and Sabin 3 strain numbering, respectively (Fig. 1) (17–19). These mutations are located in, or directly adjacent to, the reported binding sites of eIF4G and PTB on PV dV (9, 16). Impaired binding of eIF4G and eIF4B to the Sabin strains correlates with reduced PV translation and attenuation in cell-free extracts (6). Of all three mutants, the Sabin 3 mutant exhibits the most severe translation and initiation factor binding defects (5, 6). Impaired binding of PTB to the PV Sabin 3 mutant also correlates with translation attenuation (20). It is important to note, however, that these studies employed UV cross-linking of cell lysates and toeprinting assays to reveal defects in eIF4G, eIF4B, and PTB binding affinity and activity. The limitation of these nonequilibrium assays is that they cannot provide accurate affinity measurements. This makes it impossible to know the degree to which a change in initiation factor affinity to the IRES correlates with attenuation of PV translation. It will therefore be necessary to obtain quantitative affinity measurements for the interaction of eIF4G, eIF4B, and PTB with the PV IRES

This work was supported by NIGMS, National Institutes of Health Grant R01GM092927 (to C. S. F.), an American Heart Association and Myocarditis Foundation predoctoral fellowship (to B. C. A.), and by startup funds from the University at Albany, State University of New York, and the University at Albany Faculty Research Awards Program (FRAP) (to G. F.). The authors declare that they have no conflicts of interest with the contents of this article. The content is solely the responsibility of the authors and does not necessarily represent the official views of the National Institutes of Health.

[1] Both authors contributed equally to this work.
[2] To whom correspondence may be addressed. E-mail: gfuchs@albany.edu.
[3] To whom correspondence may be addressed. E-mail: csfraser@ucdavis.edu.

[4] The abbreviations used are: PV, poliovirus; IRES, internal ribosome entry site; dV, domain V; FL, fluorescein; Luc, luciferase.

© 2018 Avanzino et al. Published under exclusive license by The American Society for Biochemistry and Molecular Biology, Inc.

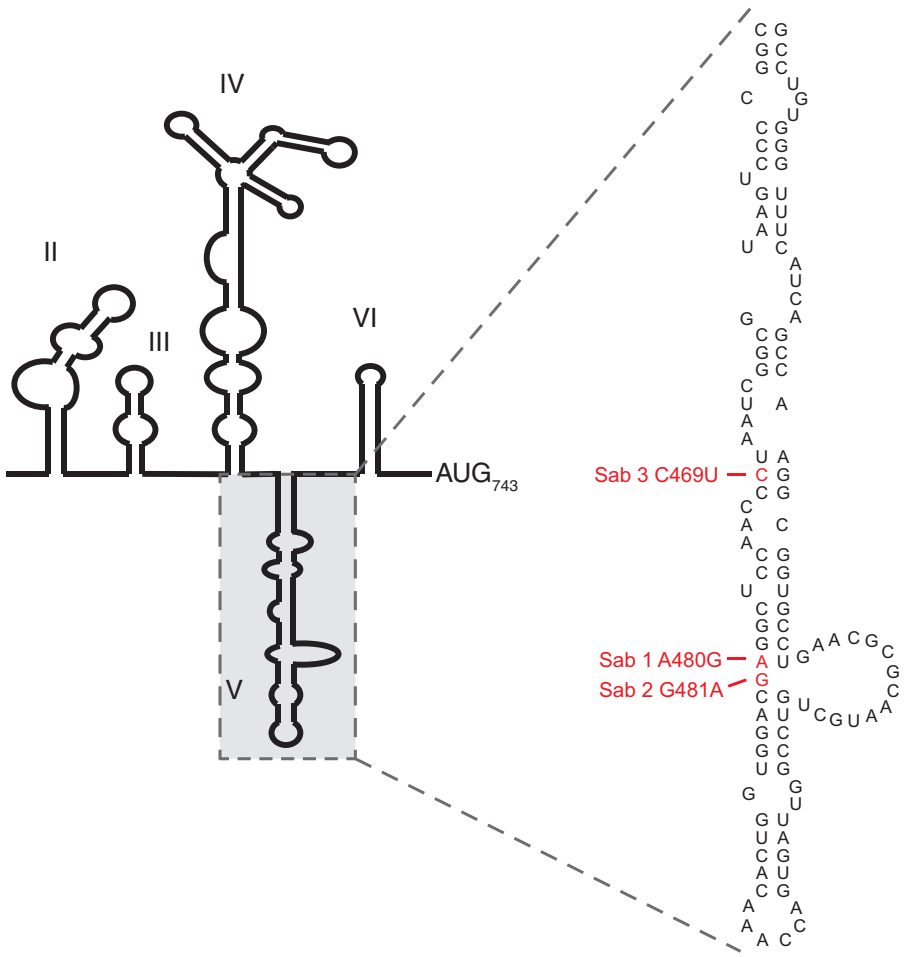

Figure 1. Schematic of the poliovirus type I Mahoney IRES secondary structure consisting of domains II to VI. Shown is the secondary structure of domain V (*shaded* and *enlarged*), with the three Sabin mutations introduced in the context of PV type I indicated in *red*.

to fully understand the extent to which the Sabin mutations reduce initiation factor affinity for the PV IRES.

Consistent with the Sabin mutants reducing the affinity of eIF4G to the PV IRES, addition of purified eIF4F to an *in vitro* cell-free lysate system can overcome the attenuation of Sabin containing PV IRESs fused to a luciferase reporter (6). Overexpression of PTB in neurons of chicken embryos can also overcome the Sabin 3 mutant defect in translation of a PV IRES reporter (20). It has therefore been suggested that variation in eIF4G and/or PTB protein levels in different cell types could provide a molecular basis for observed tissue tropism effects of Sabin mutant PV strains and reporter genes (4, 21, 22). However, it is still not entirely clear whether Sabin mutant attenuation of PV translation is absolutely restricted to cells of the central nervous system. For example, Sabin mutants have been reported to reduce PV translation and replication in cells of neuronal origin but not in HeLa cells (4, 21). In contrast, a recombinant adenovirus containing a reporter translated by a Sabin 3 mutated PV IRES is attenuated in multiple cell lines (HeLa, SY5Y, and A549) and all cell types of mice (23). This may suggest that tropism and attenuation of PV by Sabin mutants might be determined, in part, after internal ribosome entry.

Here, fluorescence-based assays have been used to overcome limitations of previous studies to further our biological insight into the mechanism by which Sabin mutants reduce translation. First, we used a fluorescent anisotropy equilibrium binding assay to directly measure the equilibrium dissociation constants of eIF4G, eIF4B, and PTB to WT and Sabin mutants in the context of PV type I Mahoney dV. Our data reveal that the Sabin mutants reduce the affinity of eIF4G and PTB for PV dV by up to 6-fold. Second, we used an IRES-dependent duplex unwinding assay to determine the impact of the Sabin mutants on the binding and activity of the eIF4G/4A/4B unwinding complex. The apparent affinity of an eIF4G/A/B unwinding complex is reduced by 2.5-fold in response to the Sabin 3 mutant. However, the Sabin 3 mutant does not alter the maximum rate of eIF4A-dependent helicase activity of the bound unwinding complex. This indicates that this mutant specifically functions by reducing the affinity of the components for the IRES rather than the activity of the bound components. To directly test this affinity model in growing cells, we overexpressed a functional truncation of eIF4GI (eIF4G$_{557–1599}$) to determine whether it can overcome the translation defect caused by the Sabin 3 mutation of a PV–luciferase replicon. Consistent with the translation of a Sabin 3 mutated PV IRES being attenuated in all cell types (23), we show that a Sabin 3 mutant PV–luciferase replicon is strongly attenuated in HeLa cells. Overexpression of eIF4G completely overcomes this

attenuation, increasing translation of the replicon to WT levels. Our results therefore provide insight into the molecular mechanism of PV Sabin attenuation and support a model in which variations in the intracellular concentration of eIF4G can be responsible for cell type–specific translation defects of a PV Sabin 3 mutant.

Results

Sabin mutations reduce the binding affinity of eIF4G to PV dV

To quantitatively measure the effects of the Sabin mutations in PV dV, we generated a fluorescence anisotropy binding assay using purified components. We introduced the Sabin 1 (A480G), Sabin 2 (G481A), and Sabin 3 (C469U) mutations in the context of the WT PV type I Mahoney sequence (Fig. 1). PV dV RNAs were 3′ end–labeled with fluorescein (PV dV-FL) as described previously and under "Experimental procedures" (24, 25). To examine the binding of each protein to PV dV, purified proteins were titrated into a fixed concentration of PV dV-FL, and the change in fluorescence anisotropy was measured. We determined the binding of PV dV-FL to two different truncations of human eIF4G: a truncation mimicking the physiologically relevant PV $2A^{pro}$ cleaved C-terminal fragment ($eIF4G_{682–1599}$) and a truncation that includes the eIF4E binding domain ($eIF4G_{557–1599}$) to provide insight into the binding of a precleaved eIF4G to the PV IRES (24). Changes in anisotropy were converted to the fraction of PV dV-FL bound at varying eIF4G concentrations and fit to a binding curve as described under "Experimental procedures."

Our data show that the equilibrium dissociation constant (K_d) of $eIF4G_{682–1599}$ for WT PV dV-FL is 75 ± 9 nM (Fig. 2, *A* and *D*, and Table 1). Introduction of the Sabin mutations substantially decreases the affinity of $eIF4G_{682–1599}$ to PV dV-FL, with the Sabin 3 mutant having the most severe binding defect with a more than 4-fold decrease in affinity (K_d = 322 ± 17 nM; Fig. 2, *A* and *D*, and Table 1). Although less dramatic, the Sabin 1 and Sabin 2 mutations have an ~2-fold decrease in affinity (Fig. 2, *A* and *D*, and Table 1). To determine the extent to which Sabin mutants affect eIF4G affinity prior to $2A^{pro}$ cleavage, we used an $eIF4G_{557–1599}$ truncation in the absence or presence of a saturating amount of eIF4E. Consistent with our previous study (24), PV dV-FL binds to $eIF4G_{557–1599}$ in the presence of eIF4E with a K_d of 40 ± 4 nM (Fig. 2, *B* and *E*, and Table 1). We show that the Sabin mutants decrease the affinity of $eIF4G_{557–1599}$ in the presence of eIF4E by up to 6-fold for the Sabin 3 mutation (Fig. 2, *B* and *E*, and Table 1). In the absence of eIF4E, the affinity of WT PV dV-FL is reduced by over 7-fold (Fig. 2, *C* and *F*, and Table 1), which is consistent with our previous data (24). The Sabin mutants reduce this affinity by up to 10-fold for the Sabin 3 mutation (Fig. 2, *C* and *F*, and Table 1). It should be noted that the affinity of the Sabin 3 mutation is an estimate based on a range of $eIF4G_{557–1599}$ from 0 to 1000 nM. These data provide quantitative evidence showing that Sabin mutations impair binding of eIF4G to PV dV by at least 6-fold prior to cleavage of eIF4G and up to 4-fold following cleavage.

In addition to eIF4G, eIF4B has been implicated in binding PV dV, and the Sabin mutations have been shown to impair binding of eIF4B to the PV IRES in cell-free extracts (6, 10). To quantitatively determine whether binding of eIF4B is directly affected by the Sabin mutations, we titrated purified recombinant eIF4B in our fluorescence anisotropy binding assay. Our results indicate eIF4B does not bind with a high affinity even to WT PV dV-FL (K_d = 4613 ± 102; Fig. 2*G* and Table 1). It should be noted that this calculated equilibrium dissociation constant is an estimated value because it is not possible to obtain a saturated complex with PV dV-FL under these conditions. Given the weak nature of the eIF4B and WT PV dV-FL interaction in our assay, we did not test the affinity of eIF4B for the Sabin mutants.

Sabin mutations impair the binding affinity of PTB to PV dV

In addition to defects in binding eIF4G, reduced binding of PTB to PV dV has been implicated as a mechanism of Sabin strain attenuation (20, 21). To determine the effect of the Sabin mutations on PTB binding, we titrated purified recombinant PTB1 (referred to hereafter as PTB) in our equilibrium fluorescence anisotropy binding assay. Our data show that PTB binds to PV dV-FL WT with high affinity, having a calculated K_d of 41 ± 4 nM (Fig. 3, *A* and *B*, and Table 1). Similar to our results with $eIF4G_{682–1599}$, binding of PTB to the Sabin 3 mutant PV dV-FL compared with WT PV dV-FL is reduced 4-fold to a K_d value of 162 ± 6 (Fig. 3, *A* and *B*, and Table 1). The Sabin 1 and Sabin 2 mutant PV dV-FL RNAs also have decreased affinities to PTB, although the effect is a more subtle (1.7-fold decreased affinity to K_d values of 72 ± 11 and 69 ± 13 nM, respectively) (Fig. 3, *A* and *B*, Table 1). These data provide quantitative evidence that the Sabin mutants impair binding of PTB to PV dV, with the Sabin 3 mutation having the most severe defect.

The stability of eIF4G, but not the unwinding activity of eIF4A, is impaired by the PV Sabin 3 mutation

Binding of eIF4G to PV dV is an important step preceding restructuring of the viral RNA by the eIF4A DEAD-box helicase. PV IRES–mediated translation is unusually dependent on eIF4A activity, as highlighted by its sensitivity to hippuristanol and dominant-negative eIF4A mutants (26, 27). In light of our data showing that the Sabin mutations in dV decrease the affinity of eIF4G to the PV IRES, we sought to determine whether the Sabin mutations also affect eIF4A-depending RNA unwinding. To examine unwinding activity on the PV IRES, we modified our fluorescent helicase assay by placing fluorescently modified molecular beacons on the 3′ side of the PV IRES (Fig. 4*A*) (24, 28). This assay allows us to accurately measure the real-time kinetics of RNA restructuring in the region downstream of the PV IRES following the authentic AUG_{743}. We chose to compare WT PV IRES to a PV IRES containing the Sabin 3 mutation in our unwinding assay because this mutation has the largest affinity change in our fluorescence anisotropy binding assay. Interestingly, at saturating concentrations of eIF4A, eIF4B, and $eIF4G_{682–1599}$, both the WT PV IRES and the Sabin 3 mutant IRES have similar unwinding kinetics (Fig. 4*B*). Each time course of unwinding was fit to a double-exponential equation to generate rate constants and amplitudes of unwinding (29). Accordingly, we only observed small changes in the rate constant of the rapid unwinding phase (k_1) and other kinetic parameters between the WT PV IRES and Sabin 3

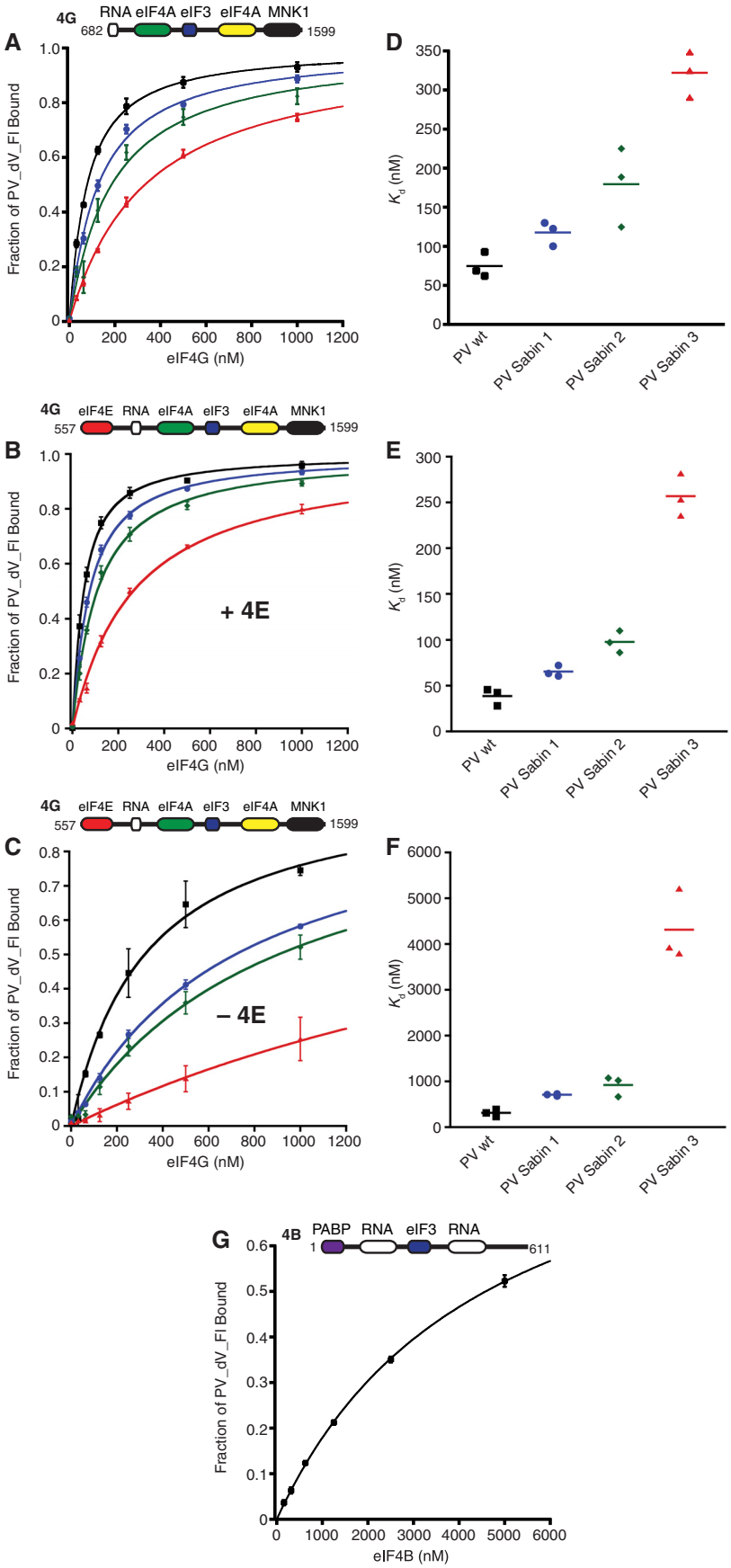
A
4G
RNA eIF4A eIF3 eIF4A MNK1
682
1599
Fraction of PV_dV_FI Bound
eIF4G (nM)
B
4G
eIF4E RNA eIF4A eIF3 eIF4A MNK1
557
1599
+ 4E
C
– 4E
D
E
F
K_d (nM)
PV wt
PV Sabin 1
PV Sabin 2
PV Sabin 3
G
4B
PABP RNA eIF3 RNA
1
611
eIF4B (nM)

Table 1
Summary of K_d and anisotropy values
All values are the mean of three independent experiments. The errors shown are standard errors.

	K_d[a]	r_{free}[b]	r_{bound}[c]	Δr_{max}[d]
	nM			
eIF4G$_{682-1599}$				
PV dV-FL WT	75 ± 9	0.122 ± 0.001	0.229 ± 0.001	0.107 ± 0.001
PV dV-FL Sabin 1	118 ± 9	0.112 ± 0.001	0.220 ± 0.002	0.108 ± 0.002
PV dV-FL Sabin 2	179 ± 29	0.113 ± 0.002	0.235 ± 0.004	0.128 ± 0.005
PV dV-FL Sabin 3	322 ± 17	0.106 ± 0.001	0.232 ± 0.001	0.127 ± 0.001
eIF4G$_{557-1599}$ + 4A + 4E				
PV dV-FL WT	40 ± 4	0.139 ± 0.005	0.232 ± 0.003	0.093 ± 0.006
PV dV-FL Sabin 1	65 ± 3	0.146 ± 0.003	0.231 ± 0.001	0.086 ± 0.003
PV dV-FL Sabin 2	98 ± 7	0.130 ± 0.002	0.229 ± 0.001	0.099 ± 0.003
PV dV-FL Sabin 3	257 ± 14	0.142 ± 0.002	0.249 ± 0.001	0.107 ± 0.001
eIF4G$_{557-1599}$ + 4A				
PV dV-FL WT	312 ± 46	0.133 ± 0.011	0.236 ± 0.003	0.103 ± 0.013
PV dV-FL Sabin 1	708 ± 15	0.112 ± 0.001	0.239 ± 0.014	0.127 ± 0.015
PV dV-FL Sabin 2#	919 ± 128	0.111 ± 0.001	0.240 ± 0.008	0.128 ± 0.008
PV dV-FL Sabin 3#	4311 ± 453	0.107 ± 0.001	0.286 ± 0.037	0.180 ± 0.034
eIF4B				
PV dV-FL WT	4613 ± 102	0.118 ± 0.001	0.346 ± 0.004	0.228 ± 0.004
PTB1				
PV dV-FL WT	41 ± 4	0.126 ± 0.003	0.265 ± 0.001	0.139 ± 0.002
PV dV-FL WT + 4G	63 ± 11	0.224 ± 0.002	0.277 ± 0.001	0.053 ± 0.001
PV dV-FL Sabin 1	72 ± 11	0.121 ± 0.002	0.264 ± 0.003	0.143 ± 0.005
PV dV-FL Sabin 2	69 ± 13	0.106 ± 0.001	0.286 ± 0.004	0.180 ± 0.003
PV dV-FL Sabin 3	162 ± 6	0.110 ± 0.001	0.277 ± 0.001	0.168 ± 0.001
PV dV-FL Sabin 3 + 4G	167 ± 39	0.200 ± 0.003	0.275 ± 0.001	0.076 ± 0.004

[a] Equilibrium dissociation constant determined by titration with the indicated protein.
[b] Anisotropy of the fluorescently labeled RNA prior to addition of protein.
[c] Anisotropy of the fluorescently labeled RNA in the protein-bound state.
[d] Difference between r_{bound} and r_{free}, representing the maximum anisotropy change.

mutant IRES (Table 2). This implies that, at saturating initiation factor concentrations, unwinding downstream of the IRES is not impaired by the introduction of the Sabin 3 mutation.

We then tested whether the apparent affinity of the eIF4G$_{682-1599}$/4A/4B complex to the IRES is altered by the Sabin 3 mutation. To examine binding of the eIF4G$_{682-1599}$/4A/4B complex in the context of our unwinding assay, duplex unwinding was measured at a fixed concentration of eIF4A and eIF4B (1 μM each) and varied concentrations of eIF4G$_{682-1599}$. Consistent with our fluorescence anisotropy results, our data revealed that the Sabin 3 RNA had a modest 2.5-fold reduced apparent affinity to the unwinding complex (eIF4G$_{682-1599}$/4A/4B) compared with the WT PV IRES ($K_{d,app}$ = 195 ± 43 and 78 ± 3 nM, respectively; Fig. 4*C* and Table 3). Analysis of our data further supports that, at saturating concentrations of eIF4A, eIF4B, and eIF4G$_{682-1599}$, the overall amplitude of unwinding and maximum initial rate of unwinding by eIF4A are similar on both the PV WT and Sabin 3 IRESs (Fig. 4, *B* and *C*, and Table 3). This strongly indicates that the Sabin 3 mutation exhibits an eIF4G binding defect but does not directly influence the unwinding activity of eIF4A when recruited to the IRES.

eIF4G and PTB binding on PV dV is not cooperative

Our fluorescence anisotropy data suggest that both eIF4G and PTB bind WT PV dV with high affinity. Previous reports using hydroxyl radical probing have suggested that eIF4G and PTB have overlapping binding sites on PV dV (9, 16). We therefore took advantage of the large anisotropy change when PTB binds PV dV to examine whether a saturating amount eIF4G$_{682-1599}$ (3 μM) influences PTB binding to PV dV. Our results show that the affinity of PTB binding is unchanged on PV dV WT in the presence or absence of saturating eIF4G$_{682-1599}$ with a K_d value of 63 ± 11 and 41 ± 4 nM, respectively (Fig. 5, *A* and *B*, and Table 1). Moreover, the affinity of PTB was also unchanged on PV dV Sabin 3 in the absence or presence of saturating eIF4G$_{682-1599}$, with a K_d value of 167 ± 39 and 162 ± 6 nM, respectively (Fig. 5, *A* and *B*, and Table 1). This suggests that the Sabin mutations do not alter the interaction between PTB and eIF4G when bound to PV dV. Taken together, our results suggest that eIF4G$_{682-1599}$ and PTB binding to PV dV is not cooperative and that binding of eIF4G does not affect PTB binding despite previous evidence for partially overlapping binding sites.

eIF4G overexpression overcomes the attenuation of PV translation by the Sabin 3 mutation in HeLa cells

The Sabin 3 mutation reduces the affinity of PV dV-FL for eIF4G$_{557-1599}$ in the presence of eIF4E by 6-fold (Fig. 2 and Table 1). The cellular concentration of eIF4G should therefore regulate the efficiency of recruitment of a Sabin 3 mutated PV genome to ribosomes. The ability of a Sabin 3 mutated PV to attenuate translation and replication in growing cells has been thought to be restricted to cells derived from the brain and spinal cord (21, 22, 30). However, the Sabin 3 mutant IRES has

Figure 2. PV Sabin mutations impair binding of eIF4G$_{682-1599}$, eIF4G$_{557-1599}$ + eIF4A + eIF4E, and eIF4G$_{557-1599}$ + eIF4A to dV. *A–C*, equilibrium binding curves of PV dV-FL WT (*black*), Sabin 1 (*blue*), Sabin 2 (*green*), and Sabin 3 (*red*) to eIF4G$_{682-1599}$ (*A*), eIF4G$_{557-1599}$ + eIF4A + eIF4E (*B*), and eIF4G$_{557-1599}$ + eIF4A (*C*), as measured by fluorescence anisotropy. The cartoon depicts binding domains in each eIF4G truncation. Each point represents the mean of three independent experiments, and *error bars* indicate standard error. *D–F*, affinity of PV dV-FL WT and Sabin mutants to eIF4G$_{682-1599}$ (*D*), eIF4G$_{557-1599}$ + eIF4A + eIF4E (*E*), and eIF4G$_{557-1599}$ + eIF4A (*F*). Values indicate K_d for the corresponding binding curves. *G*, equilibrium binding of eIF4B to PV dV-FL WT. The cartoon depicts eIF4B binding domains.

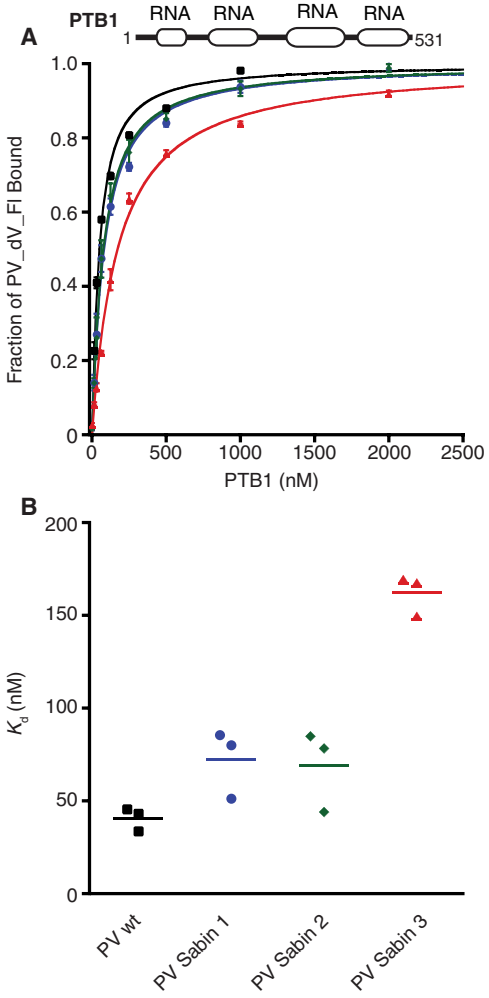

Figure 3. PV Sabin mutations impair PTB1 binding to dV. *A*, equilibrium binding of PV dV-FL WT (*black*), Sabin 1 (*blue*), Sabin 2 (*green*), and Sabin 3 (*red*) to PTB1 as measured by fluorescent anisotropy. The cartoon depicts PTB1 domains. Each point represents the mean of three independent experiments, and *error bars* indicate standard error. *B*, affinity of PV dV-FL to PTB1. Values indicate K_d for the corresponding binding curve.

been shown to be modestly attenuated (~40%) in the SY5Y, HeLa, and A549 cell lines (23). However, this study was limited by the use a chimeric adenovirus bicistronic PV IRES reporter, which may or may not reflect the regulation of a replication-competent virus. To determine whether translation of a physiologically relevant Sabin 3 mutated PV replicon is also attenuated, we used a physiologically relevant PV replicon (PV-Luc-Rep) in which the P1 region of the PV genome is replaced with a firefly luciferase reporter. This PV-Luc replicon construct contains the viral genes required for replication as well as the PV 3′ UTR and the poly(A) tail (31). We transfected WT (PV-Luc-Rep) and Sabin 3 mutated (S3-PV-Luc-Rep) PV-Luc replicon RNA into a HeLa cell line that can overexpress eIF4G$_{557-1599}$ following the addition of tetracycline (HeLa-FLAG-eIF4G$_{557-1599}$; see "Experimental procedures"). In the absence of tetracycline, out data revealed a strong attenuation of translation for S3-PV-Luc-Rep compared with PV-Luc-Rep (Fig. 6*A*). Preincubation of these cells with tetracycline for 24 h resulted in overexpression of eIF4G$_{557-1599}$ (Fig. 6*B*). Remarkably, the attenuated translation of S3-PV-Luc-Rep was completely overcome in the presence of overexpressed eIF4G$_{557-1599}$ (Fig. 6*A*). In contrast, the translation of PV-Luc-Rep was essentially unchanged following overexpression of eIF4G$_{557-1599}$. These results demonstrate that the levels of eIF4G in cells can govern the degree to which a Sabin 3 mutation can attenuate the translation of a PV replicon.

Discussion

A common feature of all three Sabin strains is the presence of a single nucleotide mutation in dV of the PV IRES that disrupts PV translation *in vitro* and in cultured cells (7, 17–19, 21, 23, 30). Impaired binding of eIF4G, eIF4B, and PTB has been observed in Sabin mutant PV IRESs and is thought to be the primary reason for reduced viral translation of Sabin strains (6, 20). However, precise affinity measurements for these components and the PV IRES have not been made, limiting our understanding of how Sabin mutants alter these important interactions. Here we used a fluorescence anisotropy equilibrium binding assay to accurately determine the affinity of eIF4G, eIF4B, and PTB to WT and Sabin mutant PV IRESs. Our data show that all three Sabin mutations impair eIF4G and PTB binding to PV dV by up to 6-fold in the case of the most inhibitory Sabin 3 mutant binding to eIF4G$_{557-1599}$ in the presence of eIF4E (Table 1). This is entirely consistent with the Sabin 3 mutation possessing the most severe defect in translational efficiency and viral infectivity (5, 6). We show that all three Sabin mutants reduce the affinity of PTB to PV dV by 4-fold (Table 1). Interestingly, the Sabin 1 and Sabin 2 mutations at nucleotide 480 and 481, respectively, are outside of the previously mapped PTB binding site, as determined by hydroxyl radical probing (16). Our data therefore suggest that the PTB1 binding site on PV dV extends several nucleotides downstream to include the Sabin 1 and Sabin 2 mutations at nucleotide 480 and 481, respectively (Fig. 7). Nevertheless, we cannot rule out the possibility that the Sabin 1 and Sabin 2 mutations induce structural changes in the IRES that indirectly alter the putative PTB binding site on PV dV. Recently, a fluorescence anisotropy assay was used as an *in vitro* screen for identifying small-molecule inhibitors of the interaction between recombinant eIF4E and eIF4G (32). We therefore anticipate that our anisotropy assay could be used in a similar way to screen for small molecules that can reduce eIF4G binding to different eIF4G-dependent IRESs. This could pave the way for an entirely new therapeutic approach to reducing the pathogenicity of eIF4G-dependent RNA viruses.

Our data reveal that eIF4B does not bind specifically to WT PV dV with a high affinity. This appears to be in contrast to previously published results of UV cross-linking experiments that mapped eIF4B binding to PV dV (6, 10). However, eIF4B binds to the eIF3 component of the 43S preinitiation complex, so it is likely that previous experiments that monitored binding in cell-free extracts observed indirect effects of eIF4B stability on the PV IRES. Nevertheless, it is also possible that other domains of the PV IRES may contribute to eIF4B binding. This would not be possible to monitor in our assay because we used a minimum PV dV for our fluorescence binding experiments. We conclude from our data that eIF4B does not have a high-affinity interaction with PV dV.

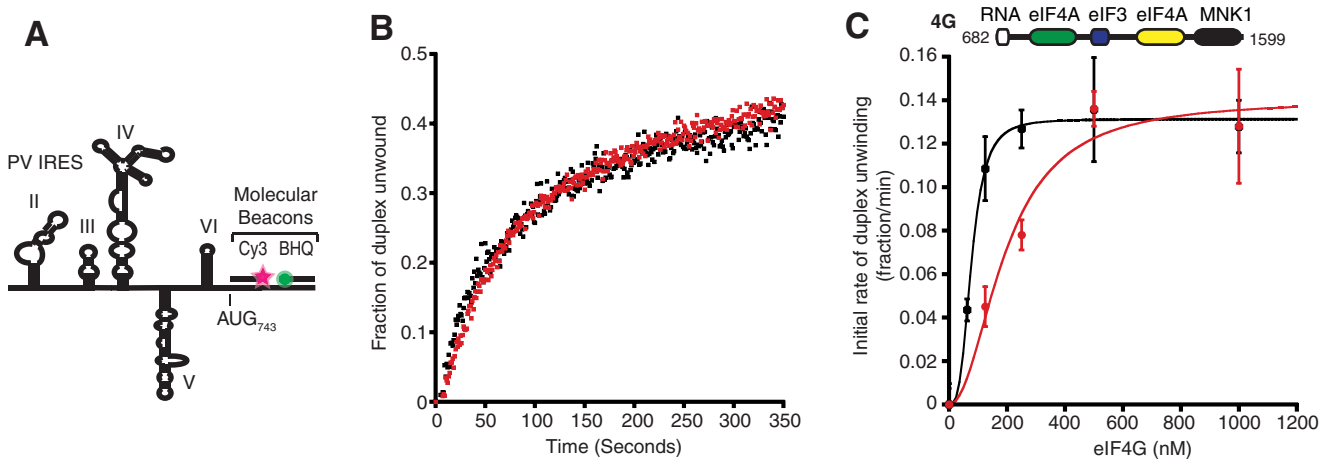

Figure 4. PV Sabin 3 mutation affects the apparent affinity of eIF4G$_{682–1599}$/4A/4B to the PV IRES. *A*, schematic depicting the PV IRES construct with the Cy3- and BHQ®-labeled RNAs used in the unwinding assay. PV IRES domains II to VI and the authentic AUG$_{743}$ are indicated. *B*, representative time course of the unwinding reaction on PV WT (*black*) or Sabin 3 (*red*). *C*, titration of eIF4G$_{682–1599}$ depicting the initial rate of duplex unwinding in the presence of 1 μM eIF4A and 1 μM eIF4B on PV WT (*black*) and Sabin 3 (*red*). The cartoon depicts the eIF4G$_{682–1599}$ domains. Data are fit to the Hill equation. Each point represents the mean of at least three independent experiments, and *error bars* indicate standard error.

Table 2

Kinetic parameters for duplex unwinding by eIF4A–eIF4B–eIF4G$_{682–1599}$

Unwinding data are fit to a double-exponential equation as described under "Experimental procedures." All values are the mean of three independent experiments. The errors shown are standard errors.

	k_1[a]	A_1[b]	k_2[c]	A_2[d]
	s^{-1}	*Fraction unwound*	s^{-1}	*Fraction unwound*
PV WT	$3.9 \times 10^{-2} \pm 1.5 \times 10^{-2}$	0.13 ± 0.04	$6.1 \times 10^{-3} \pm 9 \times 10^{-4}$	0.32 ± 0.03
PV Sabin 3	$3.2 \times 10^{-2} \pm 1.7 \times 10^{-2}$	0.18 ± 0.06	$4.3 \times 10^{-3} \pm 1.2 \times 10^{-3}$	0.27 ± 0.04

[a] Rate constant of the rapid unwinding phase.
[b] Amplitude of the rapid unwinding phase.
[c] Rate constant of the slow unwinding phase.
[d] Amplitude of the slow unwinding phase.

Table 3

Summary of $K_{d,app}$ and unwinding values

All values are the mean of three independent experiments. The errors shown are standard errors.

	$K_{d,app}$[a]	Amplitude[b]
	nM	
eIF4G$_{682–1599}$		
PV WT	78 ± 3	0.148 ± 0.02
PV Sabin3	195 ± 43	0.123 ± 0.02

[a] Apparent dissociation constant determined by titration with eIF4G$_{682–1599}$.
[b] Maximum initial rate of duplex unwinding.

An important function of eIF4G is to recruit the eIF4A DEAD-box helicase to the PV IRES. This helicase plays a critical role in inducing RNA conformational changes downstream of dV to promote ribosome recruitment (9). We employed an IRES-dependent fluorescent helicase assay to determine whether the Sabin 3 mutation reduces the rate of eIF4A-dependent duplex unwinding. Our data clearly demonstrate that the rate constant of unwinding and the amplitude of unwinding on WT and Sabin 3 IRESs are the same (Table 2). In contrast, the calculated apparent affinity of the eIF4G$_{682–1599}$/A/B complex to the Sabin 3 IRES is reduced by 2.5-fold compared with the WT IRES. This is consistent with the reduced affinity we observed for eIF4G binding to the Sabin 3 mutant PV dV using our anisotropy assay. This strongly suggests that the attenuating Sabin mutations exhibit an effect at the level of eIF4G binding but do not directly influence eIF4A-mediated RNA unwinding when eIF4A is recruited to the PV IRES. It will be important in the future to carry out a kinetic analysis of eIF4F binding to the PV IRES to determine whether the lifetime of eIF4F on the IRES is altered by the Sabin mutations. Reducing the affinity but not the activity of eIF4G/A/B is likely to be important for the function of Sabin vaccine strains, which must enable some virus to be produced to generate an immune response.

Hydroxyl radical probing experiments with PTB and the central core domain of eIF4G suggest that these proteins share partially overlapping binding sites on PV dV (9, 16). Moreover, the binding position of PTB is subtly altered in the presence of the central domain of eIF4G (amino acids 737–1116) (16). Despite this, we did not observe any change in the affinity of PTB to WT PV dV in the presence of saturating concentrations of eIF4G$_{682–1599}$. Our results therefore suggest that, despite overlapping binding sites, eIF4G and PTB do not exhibit cooperative binding to PV dV. Consistent with this, we observed no change in PTB affinity to PV Sabin 3 dV in the presence of saturating eIF4G$_{682–1599}$, suggesting that the attenuating Sabin 3 mutation does not further alter the interactions between PTB and eIF4G beyond their individual binding to PV dV.

Reduced growth and translation of PV Sabin strains has been reported in cell-free extracts and in cultured cells of neuronal origin (4, 7, 21, 30, 33). What is less clear is whether the Sabin mutants attenuate PV translation in non-neuronal cells. For example, HeLa cells have been shown to be both attenuated and nonattenuated by the Sabin mutations (20, 21, 23). It is important to note that Sabin mutated PV translation is typically monitored using a bicistronic mRNA, which may or may not reflect the rate of translation of a replication-competent PV. Never-

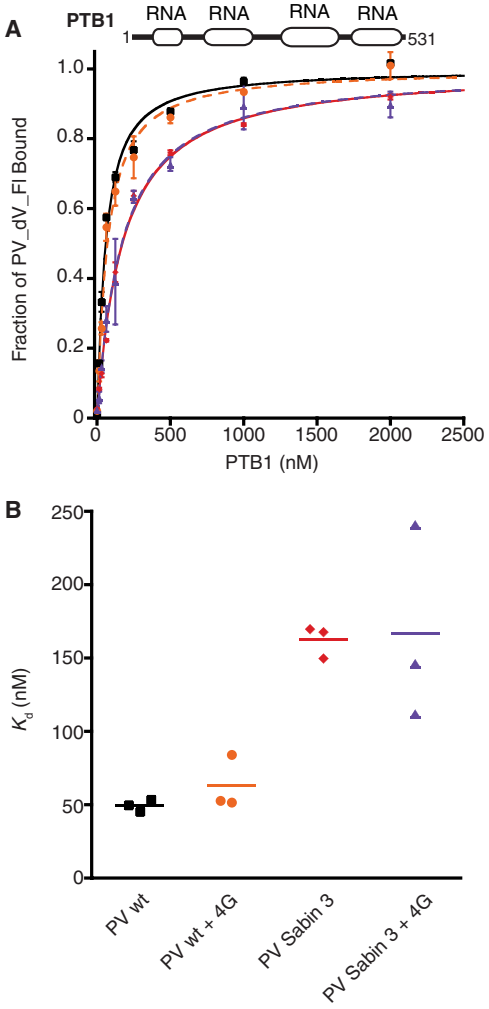

Figure 5. Binding affinity of PTB1 to PV dV is not changed in the presence of eIF4G$_{682–1599}$. *A*, equilibrium binding of PV dV-FL WT to PTB1 in the absence (*black*) or presence of 3 μM eIF4G$_{682–1599}$ (*orange*) and PV dV-FL Sabin 3 to PTB1 in the absence (*red*) or presence of 3 μM eIF4G$_{682–1599}$ (*purple*). The cartoon depicts PTB1 domains. Each point represents the mean of three independent experiments, and *error bars* represent standard error. *B*, affinity of PV dV-FL WT or Sabin 3 to PTB1 in the presence or absence of 3 μM eIF4G$_{682–1599}$. Values indicate K_d for the corresponding binding curve.

theless, the precise mechanism to explain cell-specific attenuation is not clear. One proposed explanation for PV Sabin–specific attenuation in neuronal cells is that the brain and spinal cord express lower levels of PTB than other tissues (20, 34, 35). Although the brain expresses high levels of a neural homolog of PTB (nPTB), only PTB overexpression is able to rescue the Sabin 3 translation defect of a bicistronic reporter (20). This suggests nPTB and PTB are not functionally interchangeable for stimulating PV translation and that a minimal amount of PTB is needed to promote translation.

It has been shown that addition of purified eIF4F is able to rescue the translation defect of Sabin mutant IRES reporters in cell-free extracts (6). This raises the possibility that variations in eIF4G levels in different cell types could provide one possible mechanism of cell-specific attenuation of the Sabin strains. Here, we used a physiologically relevant PV replicon to reveal very strong attenuation of translation of the Sabin 3 mutant PV replicon in HeLa cells (Fig. 6). Remarkably, this attenuation can be completely overcome by overexpressing an eIF4G truncation (eIF4G$_{557–1599}$). Interestingly, the overexpression of this eIF4G truncation did not appreciably stimulate translation of the WT PV replicon, which suggests that the levels of available endogenous eIF4G in these cells is saturating for the WT IRES. It is important to note that we used this eIF4G truncation in our work because we have rigorously characterized its activity *in vitro* and found it to accumulate particularly well in HeLa cells. It will nevertheless be interesting in the future to determine precisely whether other binding domains in eIF4G may additionally regulate PV translation. Our results suggest that the amount of endogenous eIF4G in cells may control the degree to which a Sabin 3 mutation can attenuate the translation of PV. Our findings therefore provide a plausible mechanism to explain why the degree of attenuation Sabin mutations have on PV translation varies between different cell types. Nevertheless, it is possible that the Sabin mutations also function at a later step in the virus lifecycle (23).

Interestingly, recent work has shown that a genetically modified PV can be used to specifically treat malignant glioma cells. For this application, a stable Sabin attenuated PV was made by engineering in the human rhinovirus type 2 (HRV2) eIF4G binding domain in place of PV dV (thereby preventing spontaneous reversion to WT PV) (36). As expected, the Sabin attenuated virus does not kill spinal cord motor neurons, but it effectively kills cancer cells. Many cancer cells have been shown to possess elevated levels of eIF4G. Our affinity data therefore provide, for the first time, a plausible mechanistic model to understand why this therapeutic application of PV works. We therefore anticipate that our results will be important in the development of this novel therapeutic application of PV. In addition, our quantitative assays could be used to aid the rational development of attenuating mutations in other picornaviral IRESs for basic research applications and vaccine development.

Experimental procedures

Plasmids and constructs

A pUC57 plasmid containing the poliovirus type I Mahoney IRES (PV$_{1–745}$) followed by binding sites for our previously described fluorescent unwinding reporters was generated (Genscript) (24). Plasmids containing the PV IRES with the Sabin 1, 2, and 3 mutations in domain V were cloned from the type I Mahoney IRES using the following whole plasmid mutagenesis primers: Sabin 1, 5′-CTAATCCCAACCTCGGGGCAGGTGGTCACAAACCAG-3′ and 5′-GTTTGTGACCACCTGCCCCGAGGTTGGGATTAGCCGC-3′; Sabin 2, 5′-TAATCCCAACCTCGGAACAGGTGGTCACAAACCAG-3′ and 5′-GTTTGTGACCACCTGTTCCGAGGTTGGGATTAGCCG-3′; Sabin 3, 5′-CTGAATGCGGCTAATTCCAACCTCGGAGCAGGTG-3′ and 5′-CTGCTCCGAGGTTGGAATTAGCCGCATTCAGGGGC-3′. PV dV was PCR-amplified using the primers 5′-ATCGACTCGTAATACGACTCACTATAGCGGCCCCTGAATG-3′ and 5′-CGGACACCCAAAGTAGTCGGTTCCGCC-3′. Human eIF4AI pET28c and human eIF4B pFASTBAC1 have been described previously (29). The C-terminal truncation of human eukaryotic initiation factor 4G isoform I (eIF4GI; eIF4G$_{682–1599}$) was ligated into a NdeI/XhoI

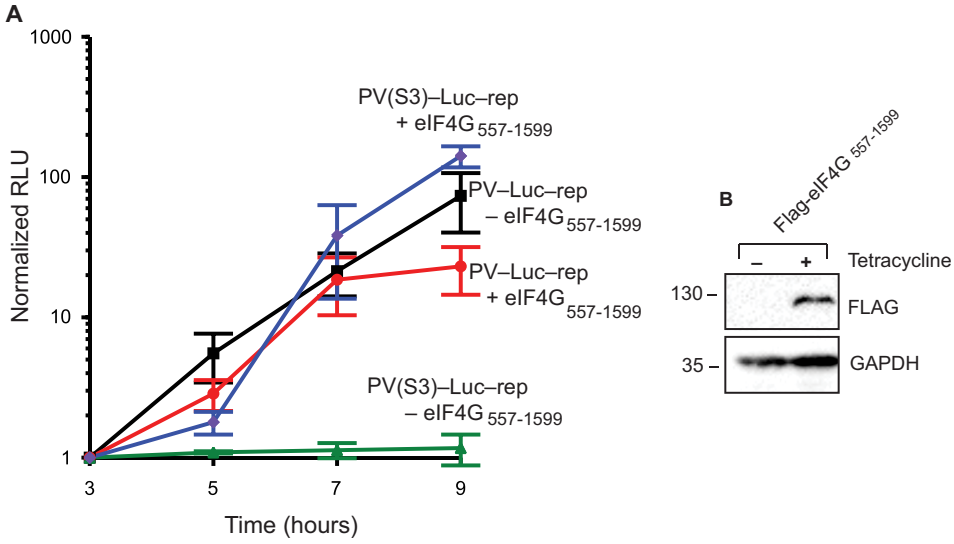

Figure 6. eIF4G overexpression stimulates the translation of a Sabin 3 mutant PV-Luc replicon RNA in HeLa cells. *A*, HeLa-FLAG-eIF4G$_{557–1599}$ cells were grown for 24 h in the absence (− *eIF4G*$_{557–1599}$) or presence (+ *eIF4G*$_{557–1599}$) of 1 μg/ml tetracycline. Cells were transfected with WT (*black* and *red lines*) or a Sabin 3 (*green* and *blue lines*) PV-Luc replicon RNA. Luciferase translation was measured 3, 5, 7, and 9 h after transfection. *Renilla* luciferase units (*RLU*) were normalized for each cell line to the 3 h after transfection measurement and plotted as *Renilla* luciferase units *versus* time as indicated. Data are the mean of three independent experiments, and *error bars* indicate S.E. *B*, tetracycline-induced expression of eIF4G$_{557–1599}$ was monitored by separating 15 μg of HeLa lysates by SDS-PAGE and Western blotting using FLAG-M2 peroxidase antibody (Sigma) and a glyceraldehyde-3-phosphate dehydrogenase (*GAPDH*)–horseradish peroxidase ^{14}C10 antibody (Cell Signaling Technology) as a loading control.

digested pET28c expression vector that has been previously modified (29).

The sequence of the C-terminal truncation of eIF4GI (eIF4G$_{557–1599}$) was previously described (37). pcDNA5/TO/FRT/FLAG was constructed by inserting the following sequence between the BamHI and NdeI sites of pcDNA5/TO/FRT: 5′-GGATCCACCATGGACTACAAAGACGATG-ACGATAAAGGTCATATG-3′). The sequence for human eIF4G$_{557–1599}$ was subcloned into pcDNA5/TO/FRT/FLAG from pFASTBAC1 using NdeI and XhoI sites to generate pcDNA5/TO/FRT/FLAG-eIF4G$_{557–1599}$ (37). PTB1 pQE was a kind gift from Anne Willis (Medical Research Council, UK). PTB1 was amplified by PCR using 5′-GAGAGACATATGGA-CGGCATTGTCC-3′ and 5′-TGTGTGCTCGAGCTAGATG-GTGGAC-3′, digested with NdeI and XhoI, and ligated into an N-terminal His–tobacco etch virus pET28c expression vector.

Stable eIF4G$_{557–1599}$ HeLa cell line

The parental HeLa R19 Flp-In TRex cell line was a kind gift from Elena Dobrikova and Matthias Gromeier (38). The stable tetracycline-inducible cell line expressing FLAG-eIF4G$_{557–1599}$ was generated according to the manufacturer's guidelines (Invitrogen). Stable cells were selected and maintained in Dulbecco's modified Eagle's medium supplemented with 5% fetal bovine serum and 2 mM glutamine in the presence of 10 μg/ml blasticidin and 100 μg/ml hygromycin.

Protein expression and purification

Human eIF4A, eIF4G$_{682–1599}$, eIF4G$_{557–1599}$, and PTB1 were expressed in *Escherichia coli* BL21 and purified as described previously (29). Human eIF4B was expressed in Sf9 insect cells as described previously (29). In general, proteins were purified by nickel-nitrilotriacetic acid Superflow (Qiagen), followed by incubation with tobacco etch virus protease to remove the His affinity tag and overnight dialysis into Hepes (pH 7.5), 100 mM KCl, 10% (v/v) glycerol, and 1 mM DTT. Human eIF4A was further purified by ion exchange (Mono Q, GE Healthcare) and size exclusion (Superdex 75, GE Healthcare) chromatography. Human eIF4G$_{682–1599}$ and eIF4G$_{557–1599}$ were further purified by HiTrap Heparin HP (GE Healthcare) and Mono Q (GE Healthcare). Human eIF4B was further purified by Mono Q (GE Healthcare) and Superdex 200 (GE Healthcare). Human PTB1 was further purified by Hi Trap Heparin HP (GE Healthcare). Following purification, proteins were concentrated using Amicon Ultra centrifugal filters (EMD Millipore) and stored at −80 °C. We found that different protein preparations generate similar data in our quantitative assays.

In vitro transcription and 3′ RNA labeling

Transcription of RNAs for fluorescence anisotropy and unwinding assays has been described previously (24, 28). Briefly, a T7 promoter was added upstream of the template DNA by PCR with appropriate primers. The PCR template was phenol-chloroform–extracted and ethanol-precipitated. RNA was transcribed using T7 RNA polymerase and phenol-chloroform–extracted and ethanol-precipitated with ammonium acetate. RNA was further purified using Sephadex G25 resin (GE Healthcare) to remove free nucleotides. RNA quality was determined using denaturing urea-PAGE.

RNA for fluorescent anisotropy assays was 3′ end–labeled with fluorescein as described previously (24, 25). Briefly, 50 μM RNA was oxidized by incubation with 15 mM sodium periodate in 100 mM sodium acetate (pH 5.2) at 37 °C for 10 min, followed by incubation at 25 °C for 30 min. Oxidized RNA was then ethanol-precipitated twice in the presence of 250 mM NaCl. Oxidized RNA was labeled by incubation with 0.5 mM fluorescein-5-thiosemicarbazide (Thermo Fisher) in 100 mM sodium acetate (pH 5.2) at 37 °C for 10 min, followed by 25 °C for 30

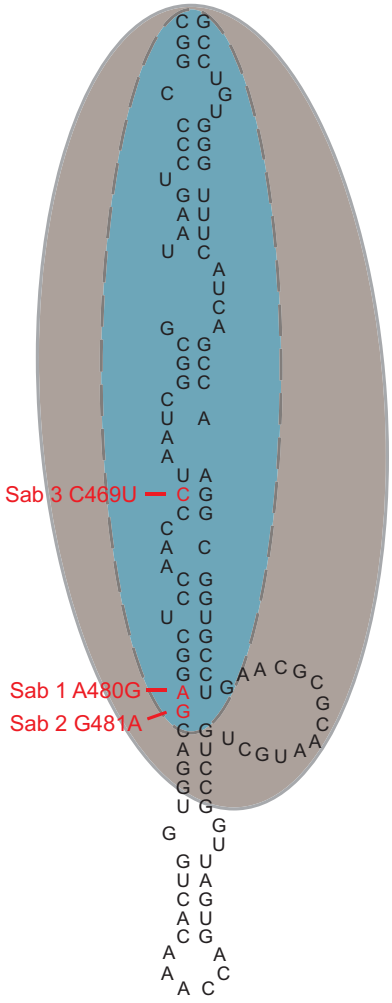

Figure 7. Refined model of eIF4G and PTB1 binding sites on PV dV. The proposed position of the central core of eIF4G (9) is indicated by the *gray oval*. The proposed position of PTB1 (16) is indicated by the *blue oval* and has been extended to cover the site of the Sabin 1 and Sabin 2 mutations.

min. Labeled RNA was ethanol-precipitated, resuspended in 100 mM Tris HCl (pH 8.0), and reduced by incubation with 50 mM $NaBH_4$ at 25 °C for 30 min. 1 M acetic acid was used to quench the reaction, which was then ethanol-precipitated. Free dye was removed, labeled RNA was purified using a Bio-Spin 6 column (Bio-Rad), and labeling efficiency was determined using a NanoDrop 2000 spectrophotometer (Thermo Fisher).

Fluorescence anisotropy binding assay

Fluorescence anisotropy was measured in a Victor X5 plate reader (PerkinElmer Life Sciences) as described previously (25, 39, 40). Reactions containing 20 nM PV dV-Fl WT or Sabin 3 were incubated with varying concentrations of $eIF4G_{682-1599}$ or PTB1 in binding buffer (20 mM Hepes (pH 7.5), 80 mM KCl, 2 mM $MgCl_2$, 1 mM DTT, 10% glycerol, and 0.1 mg/ml BSA) at 37 °C for 4 min, followed by 25 °C for 20 min. Each K_d measurement is the average of three independent experiments.

Helicase assay

Unwinding reactions were essentially performed as described previously (24, 37). Cy3 and Black Hole Quencher® (BHQ®)–labeled RNA oligos (IDT) were annealed in a 1:1:1 ratio with PV IRES template RNA containing nucleotides 1–745 of WT PV type 1 Mahoney or a mutant containing the Sabin 3 mutation, directly followed by binding sites that were complementary to our previously described 24-nt Cy3 and 19-nt BHQ® molecular beacons (24, 28). For each helicase reaction, 50 nM PV RNA was incubated with 1 μM eIF4A and eIF4B and varying concentrations of $eIF4G_{682-1599}$ in a 50-μl quartz cuvette (Starna Cells). The unwinding reaction was started by adding 2 mM Mg-ATP. All unwinding reactions were performed at 25 °C as described previously (28). Kinetic unwinding time course data were fit to a double-exponential equation, whereas initial rate data were fit to the Hill equation using KaleidaGraph (Synergy Software) as described previously (24, 29, 37). Data are the mean of three independent experiments, and error bars represent the standard error of the mean.

PV-Luc replicon transfection

The Sabin 3 mutation was introduced into prib(+)Luc-WT, the luciferase-expressing, poliovirus-derived replicon (31), with primers 5′-CCTCCGGCCCCTGAATGCGGCTAATTCCAACCTCGGAGCAGGTGGTCACAA-3′ (forward) and 5′-ATTCTTATGTAGCTCAATAGGCTCTTC-3′ (reverse) using the Q5 Site-Directed Mutagenesis Kit (New England Biolabs) and confirmed by Sanger sequencing. Following plasmid linearization with Mlu I, WT and Sabin 3 poliovirus replicon RNAs were *in vitro* transcribed with the HiScribe T7 Quick High Yield RNA Synthesis Kit (New England Biolabs) (24). The FLAG-tagged $eIF4G_{557-1599}$ HeLa cell line was grown in Dulbecco's modified Eagle's medium supplemented with 5% fetal bovine serum and 2 mM glutamine. FLAG-$eIF4G_{557-1599}$ expression was induced by addition of 1 μg/ml tetracycline (Sigma) for 24 h prior to RNA transfection. Exponentially growing HeLa cells were trypsinized, resuspended, and gently pelleted. For each transfection reaction, ~800,000 cells were resuspended in 500 μl of medium and reverse-transfected in suspension with 250 μl of Opti-MEM I, 7.5 μl of Lipofectamine 3000, and 1 μg of WT or Sabin 3 poliovirus replicon RNA following the manufacturer's transfection protocol for a 6-well plate. Aliquots of 150 μl were removed 3 h, 5 h, 7 h, and 9 h after transfection. Luminescence was measured with luciferase assay reagent (Promega) using a Glomax luminometer (Promega). To validate tetracycline-induced expression of eIF4G variants, 15 μg of HeLa lysates was separated in an 8% SDS-PAGE gel, transferred onto a nitrocellulose membrane, and detected using FLAG-M2 peroxidase antibody (Sigma) and glyceraldehyde-3-phosphate dehydrogenase–horseradish peroxidase 14C10 antibody (Cell Signaling Technology) and standard chemiluminescence methods.

Author contributions—B. C. A., G. F., and C. S. F. conceptualization; B. C. A., H. J., G. F., and C. S. F. formal analysis; B. C. A., H. J., C. M. M., and E. C. investigation; B. C. A., H. J., G. F., and C. S. F. writing-original draft; B. C. A., H. J., G. F., and C. S. F. writing-review and editing; G. F. and C. S. F. supervision; G. F. and C. S. F. funding acquisition; G. F. methodology; G. F. and C. S. F. project administration.

Acknowledgments—We thank John Hershey and members of the C. S. F. laboratory for insightful comments and critical reading of the manuscript. We thank Drs. Elena Dobrikova and Matthias Gromeier (Duke University Medical Center) for the kind gift of the HeLa Flp-In T-Rex host cell line. The prib(+)Luc-WT plasmid was a kind gift from Raul Andino University of California, San Francisco (UCSF). We thank Nancy Villa for generating the pcDNA5/TO/FRT/FLAG-eIF4G$_{557–1599}$ plasmid.

References

1. Sabin, A. B. (1985) Oral poliovirus vaccine: history of its development and use and current challenge to eliminate poliomyelitis from the world. *J. Infect. Dis.* **151,** 420–436 CrossRef Medline
2. Almond, J. W. (1987) The attenuation of poliovirus neurovirulence. *Annu. Rev. Microbiol.* **41,** 153–180 CrossRef Medline
3. Racaniello, V. R. (1988) Poliovirus neurovirulence. *Adv. Virus Res.* **34,** 217–246 CrossRef Medline
4. La Monica, N., and Racaniello, V. R. (1989) Differences in replication of attenuated and neurovirulent polioviruses in human neuroblastoma cell line SH-SY5Y. *J. Virol.* **63,** 2357–2360 Medline
5. Malnou, C. E., Werner, A., Borman, A. M., Westhof, E., and Kean, K. M. (2004) Effects of vaccine strain mutations in domain V of the internal ribosome entry segment compared in the wild-type poliovirus type 1 context. *J. Biol. Chem.* **279,** 10261–10269 CrossRef Medline
6. Ochs, K., Zeller, A., Saleh, L., Bassili, G., Song, Y., Sonntag, A., and Niepmann, M. (2003) Impaired binding of standard initiation factors mediates poliovirus translation attenuation. *J. Virol.* **77,** 115–122 CrossRef Medline
7. Svitkin, Y. V., Cammack, N., Minor, P. D., and Almond, J. W. (1990) Translation deficiency of the Sabin type 3 poliovirus genome: association with an attenuating mutation C472—U. *Virology* **175,** 103–109 CrossRef Medline
8. Svitkin, Y. V., Maslova, S. V., and Agol, V. I. (1985) The genomes of attenuated and virulent poliovirus strains differ in their *in vitro* translation efficiencies. *Virology* **147,** 243–252 CrossRef Medline
9. de Breyne, S., Yu, Y., Unbehaun, A., Pestova, T. V., and Hellen, C. U. (2009) Direct functional interaction of initiation factor eIF4G with type 1 internal ribosomal entry sites. *Proc. Natl. Acad. Sci. U.S.A.* **106,** 9197–9202 CrossRef Medline
10. Ochs, K., Saleh, L., Bassili, G., Sonntag, V. H., Zeller, A., and Niepmann, M. (2002) Interaction of translation initiation factor eIF4B with the poliovirus internal ribosome entry site. *J. Virol.* **76,** 2113–2122 CrossRef Medline
11. Hellen, C. U., Witherell, G. W., Schmid, M., Shin, S. H., Pestova, T. V., Gil, A., and Wimmer, E. (1993) A cytoplasmic 57-kDa protein that is required for translation of picornavirus RNA by internal ribosomal entry is identical to the nuclear pyrimidine tract-binding protein. *Proc. Natl. Acad. Sci. U.S.A.* **90,** 7642–7646 CrossRef Medline
12. Hunt, S. L., and Jackson, R. J. (1999) Polypyrimidine-tract binding protein (PTB) is necessary, but not sufficient, for efficient internal initiation of translation of human rhinovirus-2 RNA. *RNA* **5,** 344–359 CrossRef Medline
13. Meerovitch, K., Svitkin, Y. V., Lee, H. S., Lejbkowicz, F., Kenan, D. J., Chan, E. K., Agol, V. I., Keene, J. D., and Sonenberg, N. (1993) La autoantigen enhances and corrects aberrant translation of poliovirus RNA in reticulocyte lysate. *J. Virol.* **67,** 3798–3807 Medline
14. Blyn, L. B., Towner, J. S., Semler, B. L., and Ehrenfeld, E. (1997) Requirement of poly(rC) binding protein 2 for translation of poliovirus RNA. *J. Virol.* **71,** 6243–6246 Medline
15. Hellen, C. U., Pestova, T. V., Litterst, M., and Wimmer, E. (1994) The cellular polypeptide p57 (pyrimidine tract-binding protein) binds to multiple sites in the poliovirus 5′ nontranslated region. *J. Virol.* **68,** 941–950 Medline
16. Kafasla, P., Morgner, N., Robinson, C. V., and Jackson, R. J. (2010) Polypyrimidine tract-binding protein stimulates the poliovirus IRES by modulating eIF4G binding. *EMBO J.* **29,** 3710–3722 CrossRef Medline
17. Kawamura, N., Kohara, M., Abe, S., Komatsu, T., Tago, K., Arita, M., and Nomoto, A. (1989) Determinants in the 5′ noncoding region of poliovirus Sabin 1 RNA that influence the attenuation phenotype. *J. Virol.* **63,** 1302–1309 Medline
18. Moss, E. G., O'Neill, R. E., and Racaniello, V. R. (1989) Mapping of attenuating sequences of an avirulent poliovirus type 2 strain. *J. Virol.* **63,** 1884–1890 Medline
19. Westrop, G. D., Wareham, K. A., Evans, D. M., Dunn, G., Minor, P. D., Magrath, D. I., Taffs, F., Marsden, S., Skinner, M. A., and Schild, G. C. (1989) Genetic basis of attenuation of the Sabin type 3 oral poliovirus vaccine. *J. Virol.* **63,** 1338–1344 Medline
20. Guest, S., Pilipenko, E., Sharma, K., Chumakov, K., and Roos, R. P. (2004) Molecular mechanisms of attenuation of the Sabin strain of poliovirus type 3. *J. Virol.* **78,** 11097–11107 CrossRef Medline
21. Gutiérrez, A. L., Denova-Ocampo, M., Racaniello, V. R., and del Angel, R. M. (1997) Attenuating mutations in the poliovirus 5′ untranslated region alter its interaction with polypyrimidine tract-binding protein. *J. Virol.* **71,** 3826–3833 Medline
22. Ohka, S., and Nomoto, A. (2001) The molecular basis of poliovirus neurovirulence. *Dev. Biol. (Basel)* **105,** 51–58
23. Kauder, S. E., and Racaniello, V. R. (2004) Poliovirus tropism and attenuation are determined after internal ribosome entry. *J. Clin. Invest.* **113,** 1743–1753 CrossRef Medline
24. Avanzino, B. C., Fuchs, G., and Fraser, C. S. (2017) Cellular cap-binding protein, eIF4E, promotes picornavirus genome restructuring and translation. *Proc. Natl. Acad. Sci. U.S.A.* **114,** 9611–9616 CrossRef Medline
25. Sokabe, M., and Fraser, C. S. (2017) A helicase-independent activity of eIF4A in promoting mRNA recruitment to the human ribosome. *Proc. Natl. Acad. Sci. U.S.A.* **114,** 6304–6309 CrossRef Medline
26. Bordeleau, M. E., Mori, A., Oberer, M., Lindqvist, L., Chard, L. S., Higa, T., Belsham, G. J., Wagner, G., Tanaka, J., and Pelletier, J. (2006) Functional characterization of IRESes by an inhibitor of the RNA helicase eIF4A. *Nat. Chem. Biol.* **2,** 213–220 CrossRef Medline
27. Pause, A., Méthot, N., Svitkin, Y., Merrick, W. C., and Sonenberg, N. (1994) Dominant negative mutants of mammalian translation initiation factor eIF-4A define a critical role for eIF-4F in cap-dependent and cap-independent initiation of translation. *EMBO J.* **13,** 1205–1215 Medline
28. Özes, A. R., Feoktistova, K., Avanzino, B. C., Baldwin, E. P., and Fraser, C. S. (2014) Real-time fluorescence assays to monitor duplex unwinding and ATPase activities of helicases. *Nat. Protoc.* **9,** 1645–1661 CrossRef Medline
29. Özes, A. R., Feoktistova, K., Avanzino, B. C., and Fraser, C. S. (2011) Duplex unwinding and ATPase activities of the DEAD-box helicase eIF4A are coupled by eIF4G and eIF4B. *J. Mol. Biol.* **412,** 674–687 CrossRef Medline
30. Haller, A. A., Stewart, S. R., and Semler, B. L. (1996) Attenuation stem-loop lesions in the 5′ noncoding region of poliovirus RNA: neuronal cell-specific translation defects. *J. Virol.* **70,** 1467–1474 Medline
31. Vogt, D. A., and Andino, R. (2010) An RNA element at the 5′-end of the poliovirus genome functions as a general promoter for RNA synthesis. *PLoS Pathog.* **6,** e1000936 CrossRef Medline
32. Moerke, N. J., Aktas, H., Chen, H., Cantel, S., Reibarkh, M. Y., Fahmy, A., Gross, J. D., Degterev, A., Yuan, J., Chorev, M., Halperin, J. A., and Wagner, G. (2007) Small-molecule inhibition of the interaction between the translation initiation factors eIF4E and eIF4G. *Cell* **128,** 257–267 CrossRef Medline
33. Agol, V. I., Drozdov, S. G., Ivannikova, T. A., Kolesnikova, M. S., Korolev, M. B., and Tolskaya, E. A. (1989) Restricted growth of attenuated poliovirus strains in cultured cells of a human neuroblastoma. *J. Virol.* **63,** 4034–4038 Medline
34. Lilleväli, K., Kulla, A., and Ord, T. (2001) Comparative expression analysis of the genes encoding polypyrimidine tract binding protein (PTB) and its

neural homologue (brPTB) in prenatal and postnatal mouse brain. *Mech. Dev.* **101,** 217–220 CrossRef Medline

35. Markovtsov, V., Nikolic, J. M., Goldman, J. A., Turck, C. W., Chou, M. Y., and Black, D. L. (2000) Cooperative assembly of an hnRNP complex induced by a tissue-specific homolog of polypyrimidine tract binding protein. *Mol. Cell. Biol.* **20,** 7463–7479 CrossRef Medline
36. Goetz, C., Dobrikova, E., Shveygert, M., Dobrikov, M., and Gromeier, M. (2011) Oncolytic poliovirus against malignant glioma. *Future Virol.* **6,** 1045–1058 CrossRef Medline
37. Feoktistova, K., Tuvshintogs, E., Do, A., and Fraser, C. S. (2013) Human eIF4E promotes mRNA restructuring by stimulating eIF4A helicase activity. *Proc. Natl. Acad. Sci. U.S.A.* **110,** 13339–13344 CrossRef Medline
38. Kaiser, C., Dobrikova, E. Y., Bradrick, S. S., Shveygert, M., Herbert, J. T., and Gromeier, M. (2008) Activation of cap-independent translation by variant eukaryotic initiation factor 4G *in vivo*. *RNA* **14,** 2170–2182 CrossRef Medline
39. Sokabe, M., and Fraser, C. S. (2014) Human eukaryotic initiation factor 2 (eIF2)-GTP-Met-tRNAi ternary complex and eIF3 stabilize the 43 S preinitiation complex. *J. Biol. Chem.* **289,** 31827–31836 CrossRef Medline
40. Villa, N., Do, A., Hershey, J. W., and Fraser, C. S. (2013) Human eukaryotic initiation factor 4G (eIF4G) protein binds to eIF3c, -d, and -e to promote mRNA recruitment to the ribosome. *J. Biol. Chem.* **288,** 32932–32940 CrossRef Medline

ASBMB